On-Orbit Results and Lessons Learned from the ASTERIA Space Telescope Mission

Matthew W. Smith[1], Amanda Donner[1], Mary Knapp[2], Christopher M. Pong[1], Colin Smith[1], Jason Luu[1], Peter Di Pasquale[1], Robert L. Bocchino Jr.[1], Brian Campuzano[1], Jessica Loveland[1], Cody Colley[1], Alessandra Babuscia[1], Mary White[1], Joel Krajewski[1], Sara Seager[2]

[1]Jet Propulsion Laboratory, California Institute of Technology
4800 Oak Grove Drive, Pasadena, CA 91109; 818-354-1319
matthew.w.smith@jpl.nasa.gov

[2]Massachusetts Institute of Technology
77 Massachusetts Avenue, Cambridge, MA 02139; 617-253-6775
seager@mit.edu

ABSTRACT

The Arcsecond Space Telescope Enabling Research in Astrophysics (ASTERIA) was deployed from the International Space Station (ISS) on 20 November 2017, beginning a technology demonstration and opportunistic science mission to advance the state of the art in nanosatellite performance for astrophysical observations. The goal of ASTERIA is to achieve arcsecond-level line-of-sight pointing error and highly stable focal plane temperature control. These capabilities enable precision photometry—i.e. the careful measurement of stellar brightness over time—which in turn allows investigation of astrophysical phenomena such as transiting exoplanets. By the end of the 90-day prime mission, ASTERIA had achieved line-of-sight pointing stability of approximately 0.5 arcseconds root mean square (RMS) over 20-minute observations, pointing repeatability of 1 milliarcsecond RMS from one observation to the next, and focal plane temperature stability better than ±0.01 K over 20-minute observations. This paper presents an overview of the ASTERIA flight and ground system, summarizes the pre-delivery test campaign, and discusses the on-orbit performance obtained by the pointing and thermal control subsystems. We also describe the process for planning opportunistic science observations and present lessons learned from development and operations. Having successfully operated for over 200 days as of this writing, ASTERIA is currently in an extended mission to observe nearby bright stars for transiting exoplanets.

INTRODUCTION

The Arcsecond Space Telescope Enabling Research in Astrophysics (ASTERIA) is a 6U space telescope designed to test pointing and thermal control technologies and to perform opportunistic photometric observations of nearby stars. Developed at the Jet Propulsion Laboratory (JPL) in collaboration with the Massachusetts Institute of Technology (MIT), ASTERIA traces its roots back to the ExoplanetSat mission concept.[1-8]

The objective of ASTERIA is to demonstrate capabilities that enable photometry in a nanosatellite platform, specifically:

1) **Pointing stability.** Demonstrate optical line-of-sight pointing stability of 5 arcseconds root mean square (RMS) over a 20-minute observation and pointing repeatability of 1 arcsecond RMS from one observation to the next. By maintaining the target star image on a fraction of a pixel during an observation and from one observation to the next (i.e. from one orbital eclipse period to the next), we aim to reduce the effect of intrapixel non-uniformity on the photometric signal.

2) **Thermal stability.** Demonstrate temperature stability of ±0.01 K at a single location on the focal plane over a 20-minute observation. By controlling the focal plane temperature during observations, we aim to reduce the influence of thermal variations on orbital timescales that introduce systematic errors in the photometric signal.

3) **Photometric capability.** Demonstrate an ability to conduct at least ten 20-minute observations per day and transmit the windowed star images, plus ancillary data, to the ground for post-processing. This raw data forms the basis of photometric light curves (i.e. time series of normalized stellar intensity).

ASTERIA exceeded these objectives over the course of its 90-day prime mission. Figure 1 shows a comparison of ASTERIA's demonstrated pointing stability with that of other missions across the mass spectrum.[9] The pointing stability that ASTERIA achieved is at least an order of magnitude better than similar nanosatellites and a level of performance similar to that of larger observatories.

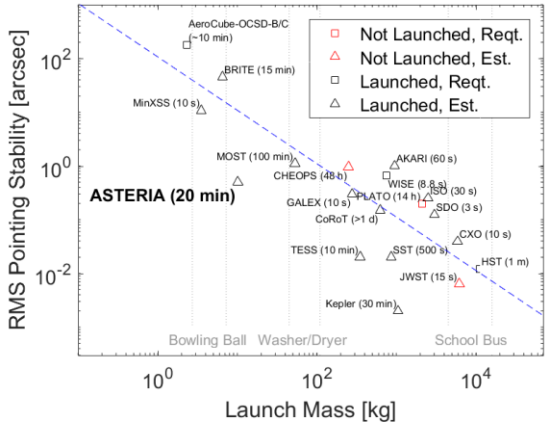

Figure 1: Pointing stability versus mass for various space missions.[9] Smaller values of RMS pointing stability correspond with better pointing performance.

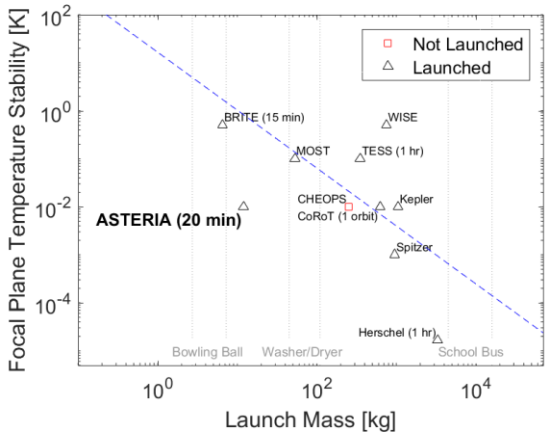

Figure 2: Focal plane temperature stability versus mass for various space missions. Smaller values of focal plane temperature stability correspond to better thermal control performance.

Similarly, Figure 2 shows the focal plane temperature stability of ASTERIA compared to Herschel[10], Spitzer[11], Kepler[12], Wide-Field Infrared Survey Explorer (WISE)[13], Transiting Exoplanet Survey Satellite (TESS)[14], Convection Rotation and Planetary Transits (CoRoT),[15] Characterising Exoplanets Satellite (CHEOPS),[16] Microvariability and Oscillations of Stars Telescope (MOST)[17], and Bright-Star Target Explorer (BRITE)[18]. ASTERIA's focal plane thermal control shows a significant improvement over the current state of the art for small spacecraft.

ASTERIA was funded by the JPL Phaeton Program, which is designed to provide flight experience and hands-on training to early career employees. The ASTERIA project kickoff was held in December 2014 and a single design review—in lieu of separate preliminary and critical design reviews—occurred in February 2016. The spacecraft was delivered to NanoRacks in June 2017, launched to the International Space Station (ISS) in August 2017 on NASA's CRS-12/ELaNa-22 mission, and deployed into orbit on 20 November 2017. ASTERIA satisfied its Level 1 requirements in February 2018, achieving full mission success, and is currently in an extended mission through August 2018. Table 1 shows a summary of ASTERIA's programmatic milestones. The total JPL budget for ASTERIA from kickoff to the end of the 90-day prime mission was $8.2M.

Table 1: ASTERIA project milestones.

Date	Milestone
11 December 2014	Project Kickoff
3 March 2015	Mission Concept Review / System Requirements Review
24-25 February 2016	Design Review
1 June 2017	Delivery to NanoRacks
14 August 2017	Launch to ISS on CRS-12
20 November 2017	Deployment from ISS
21 November 2017	Spacecraft acquisition, start of checkout
8 December 2017	Payload first image acquisition
1 February 2018	Achieved L1 requirements
18 February 2018	End of prime mission
31 August 2018	End of extended mission (plan as of this writing)

This paper will first provide an overview of the ASTERIA spacecraft design and mission operations architecture, along with a summary of the integration and test campaign prior to launch. We will then describe the on-orbit pointing and thermal performance, mission operations processes, and lessons learned.

SPACECRAFT DESIGN

ASTERIA is a 6U CubeSat (10.2 kg, 239 mm x 116 mm x 366 mm) with deployable solar arrays, 3-axis attitude control, and S-band telecommunications. As shown in Figure 4, approximately half of the internal volume is dedicated to the payload (the optical telescope assembly and payload electronics assembly) and the other half is

devoted to the spacecraft bus components (attitude determination and control subsystem, radio, electrical power subsystem, and ancillary electronics). The flight computer is physically located in the payload electronics assembly but controls all spacecraft functions.

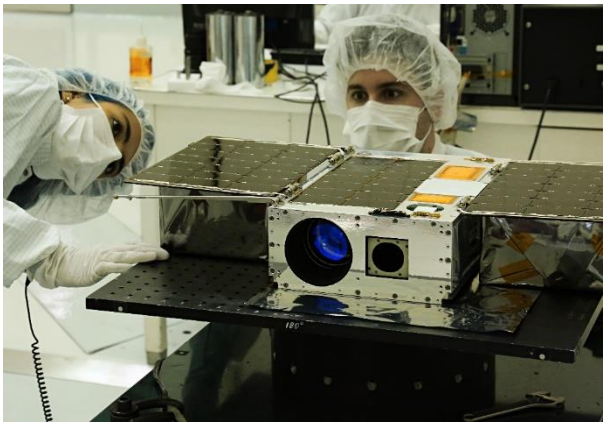

Figure 3: ASTERIA flight model with solar arrays in the deployed configuration.

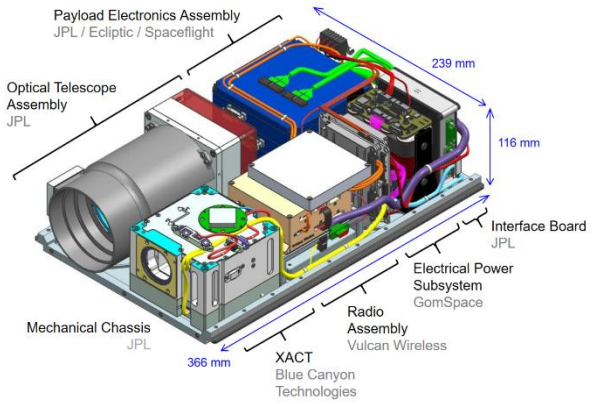

Figure 4: ASTERIA spacecraft (internal view).

Table 2: Summary of the ASTERIA spacecraft.

Parameter	Value
Mass	10.165 kg
Stowed dimensions	239 mm x 116 mm x 366 mm
Power generation	48 W (beginning of life)
Energy storage	52.7 Wh (beginning of life)
Telecom frequency	S-band
Data rates	32 kbit/s uplink 1 Mbit/s downlink
Processor	Xilinx Virtex 4FX / PowerPC405
Onboard storage	14.5 GB

Table 2 provides an overview of ASTERIA technical characteristics. The spacecraft uses a combination of commercial off-the-shelf (COTS) components, many of which are customized or modified, and components that were developed in-house. The following sections describe these subsystems in detail.

Attitude Determination and Control

ASTERIA uses the Blue Canyon Technologies (BCT) fleXible Attitude Control Technology (XACT) unit for attitude determination and control. The XACT features a star tracker, sun sensor, inertial measurement unit (IMU), magnetometer, reaction wheels, torque rods, and processor. The XACT's flight software is self-contained and capable of autonomously detumbling the spacecraft, searching for the sun, and maintaining a sun-pointed coarse attitude. Upon command, the XACT can slew to an inertial attitude and maintain 3-axis pointing with relatively high precision over long durations. The mission uses this capability during stellar observations.

Payload

The ASTERIA payload is a compact, wide field-of-view optical telescope that contains specialized hardware to perform the pointing and thermal control functions outlined above. It consists of two major subassemblies: the optical telescope assembly (OTA) and the payload electronics assembly (PEA), both shown in Figure 4.

Table 3: Summary of the ASTERIA payload.

Parameter	Value
Focal length	85 mm
Aperture diameter	60.7 mm (f/1.4)
Detector active area	2592 pixels x 2192 pixels
Pixel size	6.5 µm x 6.5 µm
Plate scale	15.8 arcseconds per pixel
Field of view	11.2° x 9.6°
Frame rate	20 Hz
Pixel bit depth	11-bits
Pass band	500 nm to 900 nm
Number of windows	8
Window size	64 pixels x 64 pixels

The OTA consists of a lens assembly, a two-axis piezoelectric nanopositioning stage, an imager, a thermal strap, and a baffle (see Figure 5). The lens assembly is a custom 5-element refractive design that is similar to a single lens reflex (SLR) camera lens but with additional features to withstand the environments of launch and low-Earth orbit (LEO). The first optic has coatings that restrict the pass band to wavelengths from 500 nm to 900 nm. The optical design, optomechanical design, assembly, and alignment were performed at JPL. The imager is a Fairchild CIS2521 frontside illuminated CMOS sensor containing 2592 by 2192 pixels, each 6.5

µm square. The imager mounts to the moving portion of the piezo stage, and the stationary portion of the piezo stage mounts to the lens assembly. This arrangement allows the imager to translate ±50 µm in the two axes orthogonal to the optical axis. The ability to translate the imager within the focal plane is optically equivalent to tip/tilt control and is used for fine pointing correction. The piezo stage is manufactured by Physik Instrumente and is a modified version of the off-the-shelf P-733.2CD model that has been customized to withstand launch and the vacuum of space.

A baffle surrounds the lens assembly and blocks stray light from the Moon and the Earth limb. A thermal strap connects the back of the imager with the baffle, providing a thermal path for rejecting heat dissipated by the imager. The thermal strap has a pyrolytic graphite film construction for the flexible section and aluminum terminals on each end. It was manufactured by Thermotive LLC.

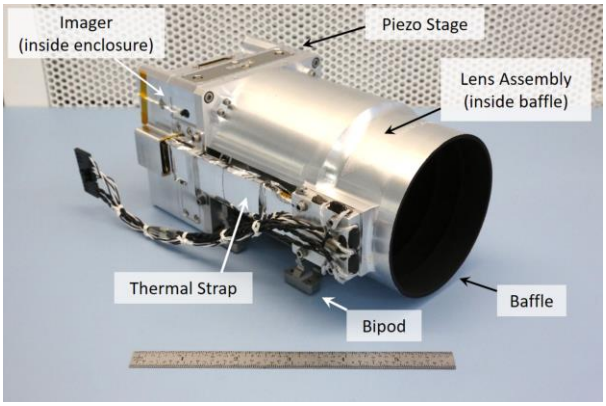

Figure 5: ASTERIA flight model optical telescope assembly (OTA).

The PEA contains the electronics required to operate the payload: the imager driver board, the flight computer, and the piezo driver board. The imager driver board was designed and manufactured by Ecliptic Enterprises and its firmware was implemented at JPL. The imager driver board is responsible for powering, configuring, and reading pixel data from the imager. It shares a custom FPGA-level interface with the flight computer that allows the transfer of image data for processing by the pointing control algorithm and storage in nonvolatile memory for later downlink.

The piezo driver board was designed at JPL and contains the electronics to create the piezo drive voltages from the raw battery bus, command the stage position, read the stage position, operate the piezo stage in closed loop using strain gauge feedback, and implement a notch filter to avoid exiting resonant frequencies in the stage.

The payload has two modes of operation: *full frame* and *windowed*. In full frame mode, the payload acquires a single image containing all pixels in the array. This captures a wide view of the sky (11.2° by 9.6°) and is used for calibration purposes. In windowed mode—the mode used for observations—up to eight windows, each with 64 x 64 pixels, are read at 20 Hz (yielding approximately 50 milliseconds of integration time). Depending on the star field, all or a subset of those windows are used by the pointing control algorithm. For photometric observations, windows from 1200 consecutive integrations are co-added onboard to form integrations covering 60 seconds.

Pointing Control Approach

ASTERIA implements a "two-stage" approach to pointing control, shown conceptually in Figure 6. During observations, the XACT points the optical boresight at the target star and maintains "coarse" attitude control for 20 minutes or more (the observation duration depends on the available orbital eclipse). In a 20 Hz control loop, windowed star images are read out of the detector and processed by a centroiding algorithm. Deviations between the measured and desired centroid locations are fed into a control algorithm that translates the piezo stage to compensate for the pointing error. The result is that the target star image remains relatively stationary with respect to the pixel boundaries. See C. M. Pong 2018 in these proceedings for a complete description of the pointing control system and on-orbit results.[9]

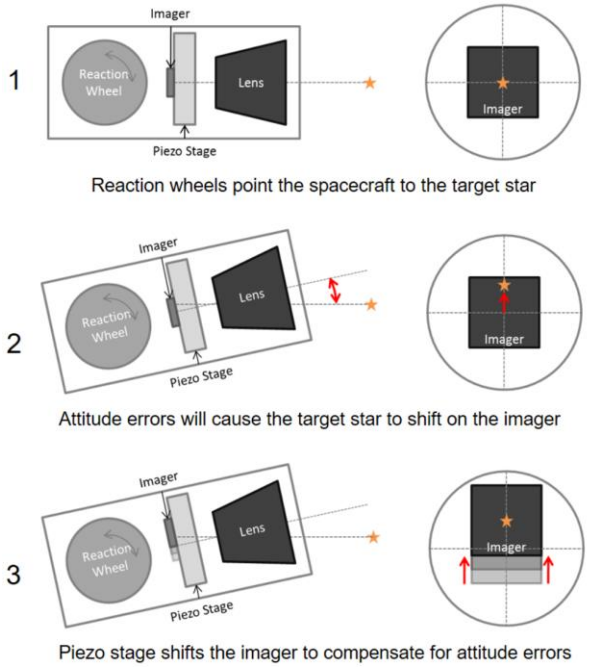

Figure 6: ASTERIA pointing control architecture.

Thermal Control Approach

ASTERIA implements a multi-layered approach to thermal control. First, the OTA is isolated as much as possible from the payload electronics and the spacecraft bus. The only connection (besides electrical wiring) between the telescope and any part of the flight system is through titanium bipods that affix the OTA to the bottom panel of the spacecraft. The estimated total conductance of the bipods is 0.015 W/K.

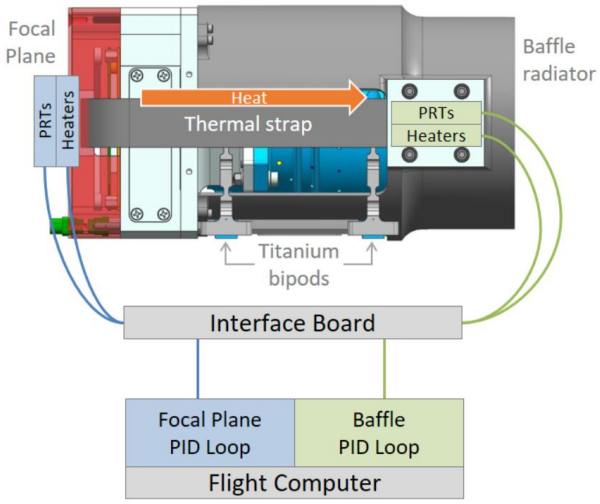

Figure 7: ASTERIA thermal control architecture.

With the OTA isolated from the rest of the spacecraft, additional layers of thermal control are implemented as shown Figure 7. The imager—located inside the red enclosure—generates over 1 W of power while operating. This heat is moved from imager through a thermal strap (~1 W/K thermal conductance) to the baffle, which acts as a radiator to space. The OTA has two active thermal control loops, one at the imager and one at the baffle end of the thermal strap. Each control loop consists of several co-located platinum resistance thermometers (PRTs) and resistive heaters. A proportional-integral-derivative (PID) controller reads the PRTs and applies small amounts of heat to maintain the desired set points at the baffle and the focal plane. The control loop around the baffle acts as a "coarse" control, compensating for relatively large environmental disturbances and controlling to ±0.5 K. The control loop around the imager acts as "fine" control, compensating for residual fluctuations and controlling to ±0.01 K.

Interface Board

This temperature control scheme relies on measuring temperature differences with very high precision. The precision sensing/control electronics are located in a single printed circuit board measuring approximately 75 mm by 65 mm developed at JPL and referred to as the Interface Board. Figure 8 shows the Interface Board in context with the flight computer and thermal control hardware.

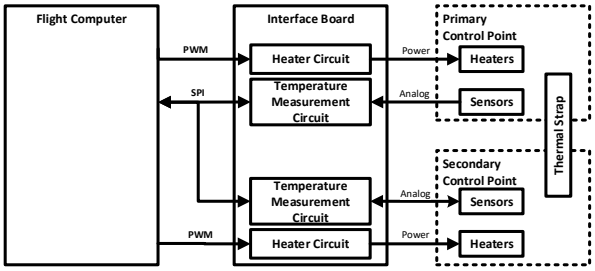

Figure 8: Precision sensing and control block diagram.

The temperature measurement circuit works by sensing the resistance in the control point PRT—located either at the imager or baffle—with respect to a high-precision calibration resistor located on the Interface Board. Two noise sources must be considered to achieve control at the level of ±0.01 K: noise in the excitation current and noise in the voltage measurement. Figure 9 shows the temperature sensitivity with respect to these two error sources. To achieve the desired level of control, the noise in the excitation must be less than a couple of nanoamps. This constraint was relaxed, however, by calibrating out the excitation error through ratio measurements against a calibration resistor.

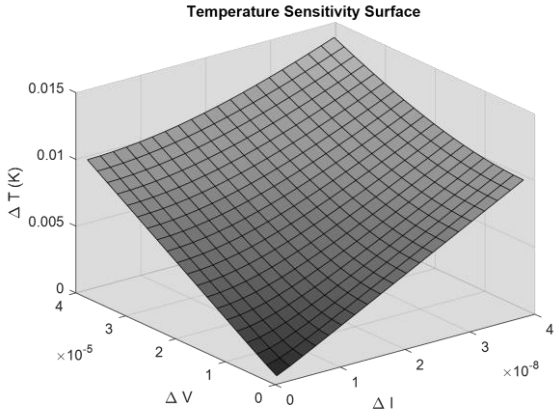

Figure 9: Sensitivity in the temperature measurement error (ΔT) to noise in the voltage (ΔV) and excitation current (ΔI).

It is critical for the calibration resistor to have a low temperature coefficient; otherwise, the temperature measurement will drift with the temperature change of the circuit board. The circuit uses a calibration resistor with a temperature coefficient of 0.002 ppm/K, compared to a minimum temperature coefficient of 0.1 ppm/K required to avoid drifts on the order of ±0.01 K

from an expected maximum temperature drift of up to ±20 K at the Interface Board mounting interface.

Command and Data Handling

ASTERIA uses the CORTEX 160 flight computer from Spaceflight Industries for onboard processing and command and data handling. It uses a Virtex 4FX FPGA with an embedded PowerPC processor running Linux. JPL modified the firmware to incorporate a custom interface with the imager driver board and to add SPI interfaces that are used to interact with subsystem components.

Flight Software

The ASTERIA flight software (FSW) uses F Prime, a free and open-source flight software framework developed at JPL and tailored to small-scale systems such as CubeSats, SmallSats, and instruments. [19] F Prime provides a software architecture based on *components* (i.e. units of FSW function similar to C++ classes) and *ports* (i.e. endpoints of connections from one component instance to another). Like classes, components have *instances* that are created when the FSW starts up.

In F Prime, FSW developers construct a high-level *model* that defines the components and ports, specifies the port connections, and defines the ground interface to FSW (e.g. the commands that FSW recognizes and the telemetry points that it generates). The F Prime tools auto-generate the following: (1) a partial C++ implementation of each component, to be completed by the developer, (2) C++ code for instantiating the components and connecting the ports, and (3) interface dictionaries for use by the ground data system.

The ASTERIA FSW consists of the following ten software subsystems that correspond to spacecraft functions: Attitude Control (including coarse pointing), Communication, Engineering, Fault Protection, Health Monitoring, Mode Management, Pointing Control (fine pointing), Power Management, Solar Array Deployment, and Thermal Control. It is written mostly in C++ (drivers for interacting with hardware are written in C) and contains around 201,000 lines of source code; 56% of these lines are auto-generated, and 25% are inherited. Several of the generic components developed for ASTERIA have been contributed back to the F Prime framework and others are in use by other missions at JPL. Developing the ASTERIA FSW required around six person-years of effort over 2.4 years.

Mode Manager

Much of ASTERIA's on-orbit functionality and behavior depends on the system mode manager and the underlying fault protection design. The high-level mode diagram is shown in Figure 10. ASTERIA has two primary modes—*Safe* and *Nominal*.

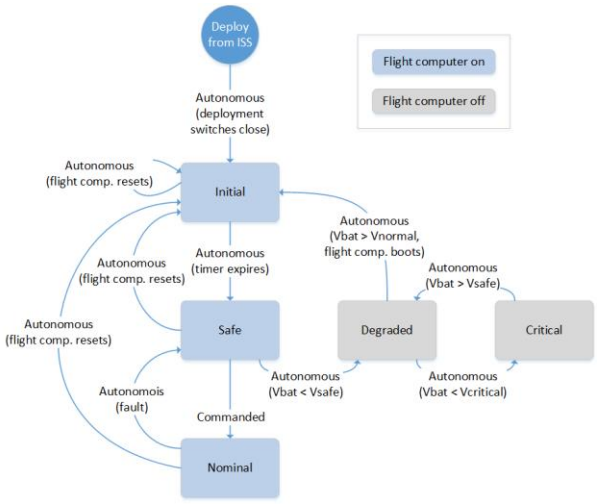

Figure 10: ASTERIA mode diagram.

Safe Mode is designed to maintain a positive energy balance across the orbital cycle (with worst-case eclipse duration) such that the spacecraft could survive for days or weeks without Earth contact. Specifically, the XACT is commanded to be in Sun Point—an internal mode that uses the sun sensor to orient the spacecraft solar panels at the Sun while in orbital daylight—and the radio is commanded into a cyclic on/off cycle that conserves energy and guarantees periodic commandability. Nominal Mode is used when executing sequences that conduct observations and perform scheduled communications passes. These operations carry somewhat higher risk than Safe Mode—for example because they rotate the spacecraft away from a Sun-pointing attitude (precluding battery charging) or operate the payload for extended periods (consuming more energy). As such, Nominal Mode activates additional layers of fault protection.

The other modes shown in Figure 10 occur in special circumstances. The spacecraft enters Initial Mode on boot, either after initial power-on following deployment form the ISS or after a flight computer power cycle. Upon deployment, Initial Mode waited for 30 minutes (as required by the ISS) before deploying the solar array and activating the other spacecraft subsystems. Following spacecraft acquisition, ground commands set onboard non-volatile flags that reconfigured Initial Mode as an immediate pass-through to Safe Mode.

Degraded Mode and Critical Mode are states governed by autonomous "load shedding" actions by the electrical power subsystem (EPS) in response to low battery voltage. The flight computer powers off in Degraded Mode and all subsystems besides the EPS power off in Critical Mode. Neither Degraded nor Critical Mode have been exercised in flight as of this writing.

Fault Protection

Fault protection is a FSW behavior that monitors the spacecraft sate and manages transitions between modes in an attempt to maintain system health and safety. The fault protection design consists of *monitors* and *responses*. Monitors periodically poll various aspects of the spacecraft state, looking for unsafe conditions. The driving philosophy behind ASTERIA's fault protection concept is to keep it simple—the monitors were chosen as catch-alls or "safety nets" that indicate a deterioration in health. Examples include low battery voltage, temperatures out of expected ranges, sequence failure, lack of FSW responsiveness, excessive time spent oriented away from the Sun, or subsystem specific health warnings.

Responses are autonomous actions triggered by monitors that reconfigure the system to achieve a known safe state. The two primary responses in ASTERIA's fault protection design are *go-to-safe* and *go-to-reset*. The go-to-safe response will (1) stop any sequence currently running, (2) power off the payload, (3) power cycle the radio and assert an on/off cycle for continued ground commandability, (4) power cycle the XACT and assert Sun Point mode, and (5) assert FSW data logging back to its default state. Go-to-safe does not invoke a power cycle of the flight computer and is therefore used in situations where there the threat to spacecraft safety is not FSW or the flight computer. For the remaining cases, fault protection will generally call the go-to-reset response, which will (1) stop any sequence currently running, (2) assert the XACT on, and (3) power cycle the flight computer. Upon boot, the flight computer will perform the go-to-safe actions while transitioning into Safe Mode.

Finally, *watchdog timers* are an important part of the fault protection architecture. These are timers that expire after a predetermined interval unless a specific action occurs to reset them. ASTERIA has three watchdog timers—a FSW health watchdog, a FSW command loss timer, and an EPS command loss timer. The FSW health watchdog resides in the EPS and will reset the flight computer if FSW fails to service the timer for a certain duration (e.g. if FSW crashes). The FSW command loss timer is automatically reset whenever the spacecraft receives a command from the ground. Once it expires, the flight computer is power cycled. The EPS command loss timer is reset via ground command. Upon expiration, performs a hard reset of all spacecraft subsystems. To date the EPS command loss timer has never expired in flight.

Power

The ASTERIA power subsystem consists of three main elements: the electrical power subsystem (EPS) card, the battery, and the solar array. The EPS card is the GomSpace NanoPower P60, which is responsible for conditioning the solar array input, regulating the battery charge/discharge cycle, and providing power to the other subsystems. The EPS outputs the raw battery voltage along with regulated 3.3V, 5V, and 12V channels. In addition to user-controlled load switching, the EPS has its own built-in fault protection. Each output switch has overcurrent protection that will power cycle the attached load if current draw exceeds a threshold (e.g. in a latchup event). The EPS also autonomously transitions between internal modes based on battery voltage. As the battery crosses user-defined voltage limits, certain subsystems are powered off to conserve the remaining charge. These cases correspond to the Degraded and Critical system modes shown in Figure 10.

The battery assembly is the GomSpace NanoPower BPX, which contains eight lithium-ion 18650 cells in series. The battery voltage varies between 24V to 32.8V—although voltages below approximately 29V have never been observed in flight—and the projected end-of-life capacity is 47 Whr. Battery sizing was based on several factors, including the amount of discharge between delivery and deployment (ASTERIA used six months as a design value), expected discharge during the initial deployment and detumble period, and the required energy storage for observations during orbit eclipse.

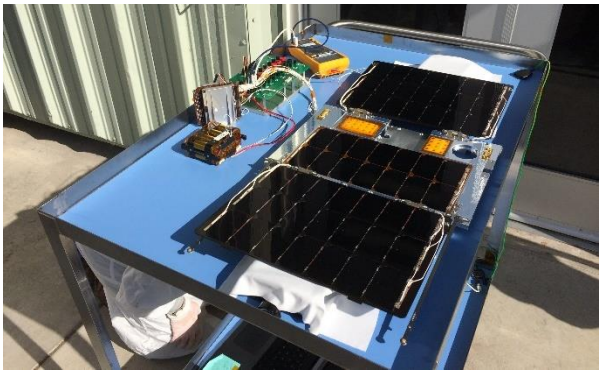

Figure 11: Testing the ASTERIA solar array under natural illumination.

The solar array was sourced from MMA Design LLC and consists of two deployable panels plus cells incorporated into the top panel of the spacecraft (Figure

11). The array contains eight strings, each consisting of seven SpectroLab UTJ cell-interconnect-coverglass (CIC) modules. The deployable panels are spring loaded and are held in place during launch with dedicated restraints that do not rely on the dispenser to maintain the stowed configuration.

Telecommunications

The ASTERIA telecommunication subsystem uses S-band for uplink and downlink. The flight element consists of a full duplex software-defined transceiver and two low-gain patch antennas on opposite surfaces of the spacecraft to enable contact while spinning. These components were manufactured by Vulcan Wireless.

The transceiver includes an internal switch to select which of the two antennas is active. It also features a diplexer to split uplink and downlink, a solid-state power amplifier, and a low-noise amplifier. The two patch antennas are identical and work at both the transmit and receive frequencies. ASTERIA uses two sets of data rates, one for Safe Mode and one for Nominal Mode. The Safe Mode data rates are 4 kbit/s uplink and 10 kbit/s downlink, and the Nominal Mode data rates are 32 kbit/s uplink and 1 Mbit/s downlink.

Figure 12: 21-meter antenna at Morehead State University. Image credit: Morehead State University Space Science Center.

The ground element consists of a 21-meter diameter parabolic antenna at Morehead State University in Kentucky (Figure 12)[21] and an AMERGINT softFEP-9000 modem. For cost reasons, ASTERIA does not have a backup ground station and is wholly reliant on the station at Morehead State University. To date, service availability—i.e. percentage of scheduled passes successfully executed, accounting for weather outages—has been better than 97%.

Structure

The spacecraft mechanical chassis was designed at JPL in conformance with the NanoRacks 6U deployer ICD. Instead of the four "rails" on each corner used by the traditional P-POD design,[20] the NanoRacks specification relies on two "tabs" that run along the long edges of the spacecraft and engage with C-shaped channels in the dispenser. For ASTERIA, these two tabs were on either edge of a bottom plate to which nearly all of the internal components mounted (shown in Figure 4). By mounting components to the bottom plate, we were able to maintain accessibility to the individual subsystems and their electrical connections during spacecraft build-up. This mounting scheme also had the advantage of allowing the components to sink heat into the spacecraft chassis (see below).

Spacecraft Thermal Design

To achieve the payload temperature control objective, ASTERIA required two separate but non-independent thermal designs: a design for focal plane temperature stability (described above) and the system-level thermal design. At the system level, the important inputs were the power dissipation in each operational mode and the environment. The maximum orbit-average power dissipation was 24 W, corresponding to Safe Mode operation in full sunlight. The internal dissipations and external loads (e.g. solar flux, Earth albedo) were inputs to a Thermal Desktop model that was used to evaluate surface treatments and other design decisions that maintain components at safe temperatures over the range of possible operational and environmental conditions.

A significant driver of the thermal design was the inclusion of body-mounted solar panels, which impart a non-trivial thermal load on the spacecraft when illuminated. The combination of this and other internal dissipations, and environmental loads, led to a surface coating of 10-mil silver Teflon over nearly the entire exposed surface of the spacecraft. All the chassis walls were well connected thermally, so the entire spacecraft body served as a "radiator." The components with high power dissipation (flight computer, payload electronics, radio) were purposefully well-coupled to the bottom plate. The telescope, the batteries and the interface board were thermally isolated from the bottom plate using titanium bipods for the telescope and low conductivity polymer spacers for the batteries and interface board. The batteries were isolated in order to avoid reaching the low-temperature limit during a worst-case deployment, and the Interface Board was isolated to reduce the amplitude of the temperature disturbance on the temperature-sensing circuitry.

INTEGRATION AND TEST CAMPAIGN

Due to the budget and schedule limitations that accompany a project of this scope, ASTERIA was not able to complete the exhaustive battery of tests that typically occur on large-scale JPL flight projects. On the other hand, the project wanted to ensure a reasonable chance of success within the expectations of our risk posture. As such, ASTERIA embarked on a tailored set of tests at the subsystem and system level to verify components, validate the design, and demonstrate robustness to environments and scenarios. Much of the system-level integration and functional testing occurred in the JPL Integrated CubeSat Development Laboratory (ICDL, Figure 13).

Figure 13: ASTERIA integration and test venue in the JPL Integrated CubeSat Development Laboratory (ICDL).

Subsystem Tests

The complete tally of subsystem level tests is too numerous to list here, and many tests were of the more mundane (but essential) functional checkout or electrical integration variety. However, there are a handful that merit additional discussion.

Development of the thermal control system required incremental testing and validation of the hardware elements. One important test was verifying that the temperature measured by the Interface Board was independent of the temperature of the board itself (since the board is attached to a thermally fluctuating spacecraft chassis). Figure 14 shows test results reading the pseudo-temperature of a thermally stable 1000-ohm resistor while changing the temperature of the Interface Board. Reading a resistor instead of a temperature sensor is an effective way to evaluate the board's ability to perform measurements because the pseudo-temperature reading should be constant. Any fluctuations in the measurement are considered noise. The test showed that the board has a measurement precision of ±0.005 K over a board temperature fluctuation of 13 K.

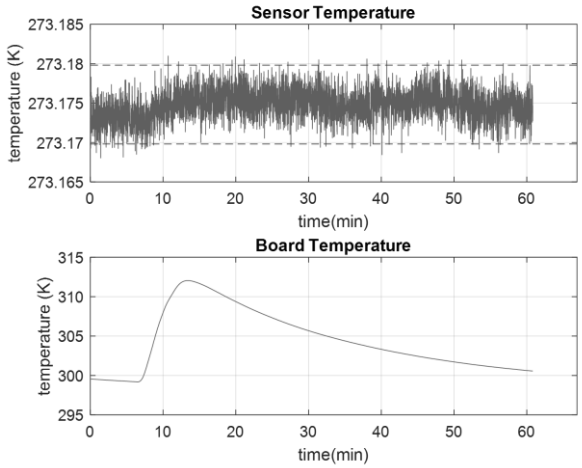

Figure 14: Temperature measurement is insensitive to the temperature of the Interface Board.

In addition, the Interface Board temperature measurement was compared to a measurement produced by calibrated laboratory equipment. Figure 15 shows the temperature measured by co-located sensors, one read by the Interface Board and one read by a Lakeshore model 340 Temperature Controller. The Interface board measurement closely matches that of the laboratory equipment.

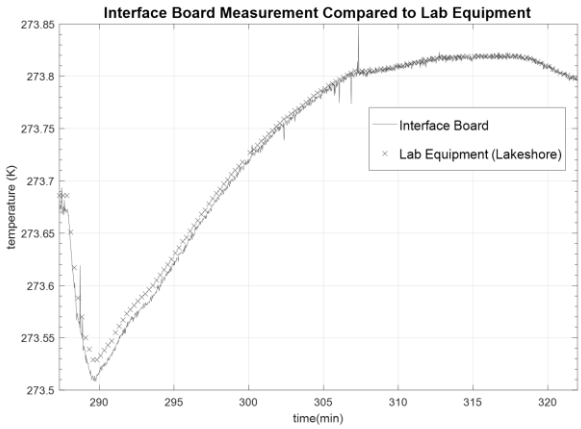

Figure 15: Comparing temperature measurements by the ASTERIA Interface Board and laboratory equipment (Lakeshore 340).

Another important test was verifying the alignment of the optical telescope assembly in flight-like environmental conditions. The OTA was placed in a thermal vacuum chamber and subjected to temperatures varying over the expected on-orbit range of ±20°C (see Figure 16). A collimated laser was projected into the chamber and the optical point spread function (PSF) was

captured as the pressure and temperature varied. The measured PSF compared favorably with numerical predictions.

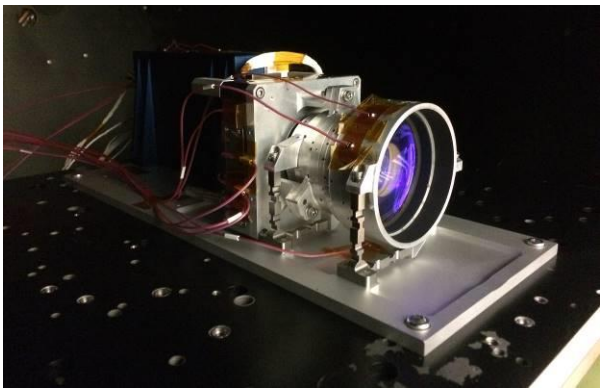

Figure 16: Optical telescope assembly (without baffle) in a thermal vacuum chamber, instrumented with thermocouples.

The cells on ASTERIA's solar array are covered while in the stowed configuration. Therefore, given the criticality of solar array deployment and historical reliability issues for CubeSat mechanisms, the project performed an early risk-reduction test by demonstrating solar array deployment under thermal vacuum conditions. A solar array engineering development unit (EDU) was placed on a test stand in a thermal vacuum chamber. After evacuating the chamber and cooling the array to –75°C, the deployment mechanism was activated and the panels deployed within three seconds, as intended.

A series of tests were conducted to validate the end-to-end information system. Prior to integration with the spacecraft, the flight radio was transported to Morehead State University for compatibility tests with the 21-meter antenna and associated ground station equipment. A separate set of tests at JPL verified the interface between the flight radio, ground modem (which was resident at JPL during the development phase), and mission operations software. After spacecraft delivery but before deployment, the ground modem was relocated to Kentucky for integration with the antenna facility. After that, a final "thread test" verified the flow of data from the ground station to the ASTERIA operations center, through the operations console, and into the archive server.

Environmental Tests

The ASTERIA spacecraft underwent a tailored set of environmental tests. One of the most resource-intensive but valuable of these was the system thermal vacuum test. The objectives were to correlate the system thermal model, demonstrate focal plane control with representative disturbances, verify system functionality at hot and cold extremes, and perform several thermal cycles to verify workmanship. Most subsystems were integrated into the vehicle for this test, with the notable exception of the solar array. Instead, a test-specific spacecraft top plate was installed that contained a patch heater in place of the body-mounted solar cells. This heater was sized to match the estimated heat load transmitted into the spacecraft body when the cells are illuminated. Boundary conditions—including the chamber walls and the aforementioned patch heater—were varied throughout the test as needed. The test took place over 220 hours in vacuum and accomplished all objectives, including uncovering previously untested fault scenarios related to hardware behavior at extreme temperatures.

ASTERIA underwent mass property testing using a KGR500 to determine the flight system mass and moments of inertia[22]. This test verified that the center of mass was within the limits required for momentum control and produced refined values for use in attitude control simulations.

The final two tests were random vibration testing—the only system-level environmental test required by NanoRacks—and measurement of the residual magnetic dipole of the spacecraft. The measured residual dipole was higher than expected. The origin of this finding is not fully understood, given that no dipole measurement was conducted prior to vibration testing and the spacecraft has little ferrous material. Flight workarounds have been developed to mitigate this effect. [9]

Fault Protection Tests

Thorough fault protection testing was a critical activity during the system integration and test campaign. The highest priority fault monitors and responses were exhaustively tested on the "FlatSat"—a benchtop emulator of the spacecraft hardware and software—and ultimately on the flight system itself.

Mission Scenario Tests

Validating the system-level functionality, behavior, and robustness was the main objective of the ASTERIA mission scenario test (MST) campaign. As the final spacecraft hardware and software came together, the team exercised flight-like scenarios that were considered critical to accomplishing the mission. These tests exercised complex subsystem interactions and uncovered latent "emergent behavior" that was not observed when components were operated in isolation. In a few cases, the MST results forced relatively late-breaking but nonetheless essential updates to FSW and default parameters. The MSTs were as follows:

- *Nominal deployment.* This test validated autonomous behaviors that occur during the critical time between ejection from the ISS and initial ground acquisition (i.e. 30 minute timer, solar array deployment, Safe Mode entry, detumble, sun acquisition, radio initialization, first ground contact). Also used to validate final flight parameters.

- *Off-nominal deployment.* This test was similar to the nominal deployment scenario but added worst-case timeouts, faults, and off-nominal events.

- *Nominal day-in-the-life.* This test verified behaviors needed for typical mission operations such as communication passes, sequenced operations, and file maintenance.

- *Off-nominal day-in-the-life.* This test was similar to the nominal day-in-the-life but with various fault injections (e.g. sequence failure, low battery voltage).

- *FSW update.* This test verified the ability to uplink a new software image over the radio link, remotely boot into the new FSW version, and revert back to the original version.

- *Nominal observation day-in-the-life.* This test exercised the end-to-end payload functionality, including optical stimulation with a star simulator, closing the piezo stage control loop for multiple 20-minute observations, recording and co-adding windowed images, and downlinking the images over the radio link.

Operational Readiness Tests

Shortly after delivery of the spacecraft, the ASTERIA team conducted an operational readiness test (ORT) to validate the mission operations system—its tools, processes, and interfaces—and to prepare the team for the tempo and demands of operations. The ORT lasted four days and emulated deployment and subsystem checkout, albeit on a compressed timeline relative to the real mission to maximize training. The "FlatSat" testbed served as a stand-in for the flight system. Commands and telemetry flowed between the operations console and the testbed (located in a separate building) over a path that included the ground station modem and a radio frequency link.

The ORT had a few key limitations. First, the testbed was unable to emulate the variation in radio signal strength that occurs when the spacecraft slowly rotates (as designed) during orbital eclipse while in Safe Mode. During actual operations, this caused a reduction in command uplink and data downlink efficiency during night-time passes. The team accepted this risk when scoping the ORT. We developed methods of mitigating the issue that were exercised in flight (e.g. maintaining a constant attitude during eclipse and pointing the spacecraft antenna at the ground station during passes). Another testbed limitation was a lack of synchronization between the orbit simulation, provided by the BCT Realtime Dynamics Processor (RDP), and the simulated solar array input, provided by a laboratory power supply. This prevented the team from fully exercising fault scenarios at the intersection of attitude control and power during the ORT (e.g. low battery voltage caused by loss of Sun pointing). The team accepted this risk based on the fact that monitors and responses related to these scenarios had been thoroughly tested on the flight vehicle before delivery.

Holding the ORT shortly after delivery achieved a useful balance of (1) allowing the team to focus on completing integration and testing of the flight vehicle and (2) having the team available before they dispersed to other projects during the multi-month wait between delivery and deployment. A few weeks prior to deployment, the team held a "refresher" ORT to become reacquainted with the lessons learned by the first ORT.

MISSION OPERATIONS AND RESULTS

ASTERIA's mission began on 20 November 2017 at 12:25:01 UTC when it was deployed into low-Earth orbit (LEO) from the ISS (see Figure 17). This section describes operations during the prime mission, including deployment, acquisition, commissioning, and results of the pointing and thermal control technology demonstrations. We also discuss the selection of targets for opportunistic science and the observation planning process.

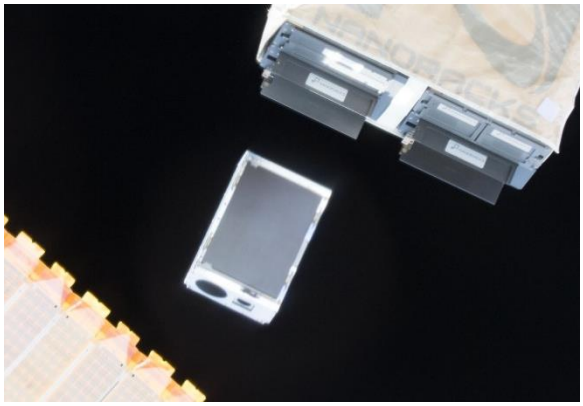

Figure 17: ASTERIA deploying from the ISS. Seen at the bottom left is a section of the ISS solar array in the background. Image credit: NASA.

Orbit Geometry and Operational Impacts

Mission operations are strongly influenced by orbital geometry and the resulting patterns in eclipse timing and communication pass opportunities. ASTERIA has no propulsion and therefore resides in a similar orbit to the ISS—approximately 400 km altitude, 51.6° inclination. The orbital period is 92.6 minutes and the eclipse duration varies as a function of the beta angle (β), the angle between the orbit plane and the Earth-Sun vector. The value of β varies between 0° and 75° over the course of several weeks as the orbit slowly precesses. When β=0°, the orbit plane is coincident with the Earth-Sun vector and the eclipse duration is 35.8 minutes, its maximum value. Conversely, when β=75°, the orbit plane is nearly orthogonal to the Earth-Sun vector and the spacecraft is in daylight throughout the entire orbit (eclipse duration is zero). Figure 18 shows ASTERIA's beta angle and eclipse duration during the prime mission.

To mitigate the effects of stray light, observations only occur during eclipse. Periods of low beta angle (long eclipse) are advantageous because they maximize viable observation time per orbit. On the other hand, these periods are more stressing on the power subsystem because the time spent in sunlight is a minimum. This relative lack of sunlight also causes reduced component temperatures that, if not properly managed, may violate allowable flight temperature (AFT) limits. Periods of high beta angle are also somewhat problematic, but for different reasons. High beta angles preclude observation (since there is no eclipse) and result in higher component temperatures due to the constant solar loading.

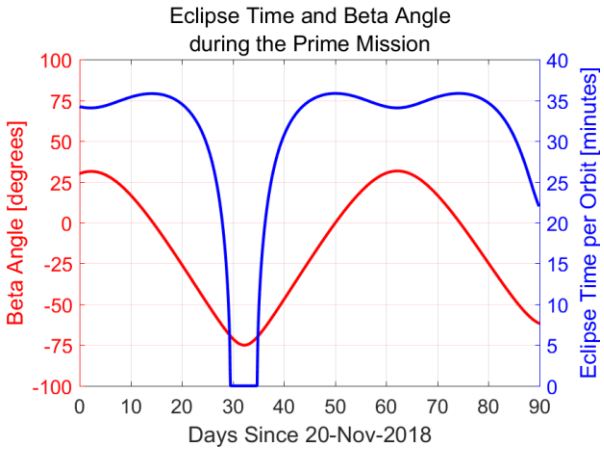

Figure 18: Beta angle and eclipse times during the ASTERIA prime mission.

Orbit geometry also has a strong influence on communication opportunities. ASTERIA completes 15 orbits per day. Of those, six generally overfly the ground station at Morehead State University and are therefore geometrically capable of supporting communication passes (see Figure 19). Each pass lasts eight to ten minutes, and the maximum elevation as seen from the ground station varies dramatically. Of the six passes available per day, the first two are usually at higher elevation, the middle two are usually at low elevation, and the last two are at high elevation again. During routine operations, the ASTERIA ops team selects one high-elevation pair of passes per day, the choice driven by the local time of the passes at JPL and at Morehead State University.

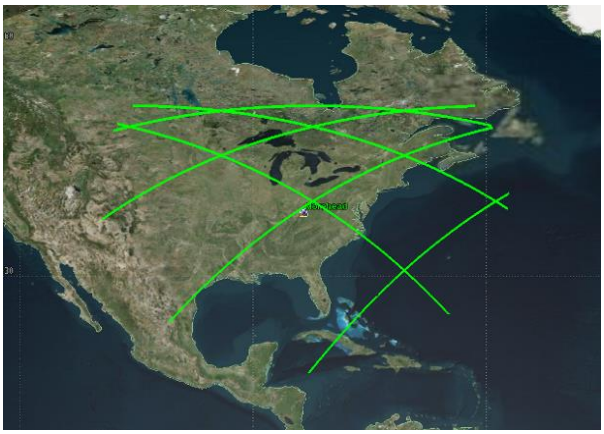

Figure 19: ASTERIA ground tracks during a typical set of six daily passes over the ground station at Morehead State University in Kentucky.

Mission Operations System

The core of the ASTERIA mission operations system (MOS) is an adapted version of the WISE Telemetry Command and Communications Subsystem (WTCCS).[23] It is a software suite that provides capabilities for translation and transmission of commands; uplink of files; downlink of telemetry, log messages, and files; and automation of each listed capability through a TCL API. WTCCS has been augmented by a set of ASTERIA-developed Python scripts that catalog downlinked files and push the data to a server for team access. An instance of OpenMCT[24]—a flexible, open source viewer designed for mission operations—allows team members to quickly plot and analyze spacecraft health and safety telemetry as a function of time, view GDS logs, view raw file and telemetry downlink, and create command products to downlink telemetry. Additionally, plotted telemetry may be exported as PNG or JPG files, and queried telemetry may be exported in CSV, JSON, or tab-delimited formats for more detailed analysis.

The ASTERIA operations team for the first few weeks of the mission consisted of seven to ten JPL staff members (depending on the activity) plus one MIT

science team member co-located at JPL. As commissioning activities concluded, the team tapered down to 2.5 full-time equivalent JPL staff and one MIT science team member, where it remained for the rest of the prime mission. The ground station operators at Morehead State University consist of a half-dozen talented students who rotate through shifts.

ASTERIA operations take place in the JPL Earth Orbiting Mission Operations Center (see Figure 20). During routine operation, passes generally consist of acquiring the spacecraft carrier as it rises into view of the ground station, uplinking and initiating a new sequence (e.g. to conduct an observation or schedule future passes), downlinking images and recorded engineering telemetry, and performing file maintenance (e.g. deleting previously downlinked data). The operations team uses Two-Line Element (TLE) sets from the Joint Space Operations Command (JSpOC) for orbit prediction and pass planning.

Figure 20: ASTERIA operations in the JPL Earth Orbiting Mission Operations Center.

Deployment, Acquisition, and Commissioning

Unlike most CubeSats deployed from the ISS, ASTERIA—and the other CubeSats in our airlock cycle—deployed into space individually and with a 3-hour plus gap between each deployment. We therefore avoided the tracking ambiguities often associated with simultaneous ISS deployments. ASTERIA's TLE was available within 12 hours of deployment.

The first attempt at contact occurred on 22 November 2017 at 00:39 UTC (approximately 36 hours after deployment). This attempt was unsuccessful because—as later determined via recorded telemetry—the radio on/off cycle in Safe Mode was, coincidentally, in the off state during the first pass. Approximately 90 minutes later, during the second pass of the mission, the operations team made initial contact with ASTERIA and received on-orbit telemetry for the first time via the Morehead State University ground station.

Data downlinked in the mission's opening days confirmed that the deployment logic had executed as desired, including the required 30-minute powered-off period immediately after ejection from the ISS, followed by solar array deployment, detumble, and sun acquisition. The initial tip-off rates were less than 1 degree per second in all three axes. The low initial rates combined with ASTERIA's deployment into orbital daylight allowed the XACT to find, acquire, and settle in a Sun-pointed attitude within 150 seconds.[9]

The first week of the mission was dedicated to checking out the spacecraft subsystems and evaluating the on-orbit performance against pre-launch predictions. Results for the power subsystem are shown in Figure 21 and Figure 22 below. The on-orbit maximum battery voltage was very close to the predicted value (within 0.13V). The on-orbit measured solar array power was approximately 5W greater than the predicted value, excluding periods of transition into or out of eclipse.

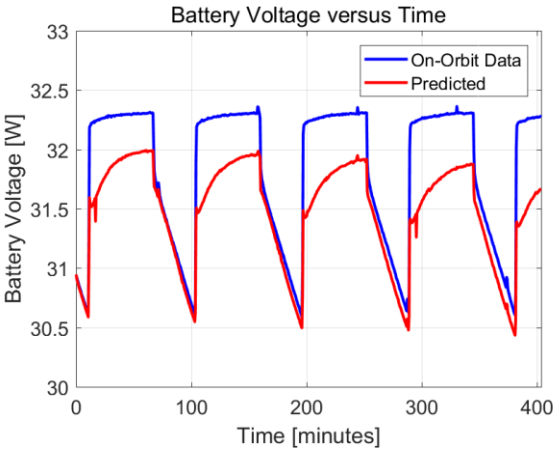

Figure 21: Measured and predicted battery voltage over several orbits.

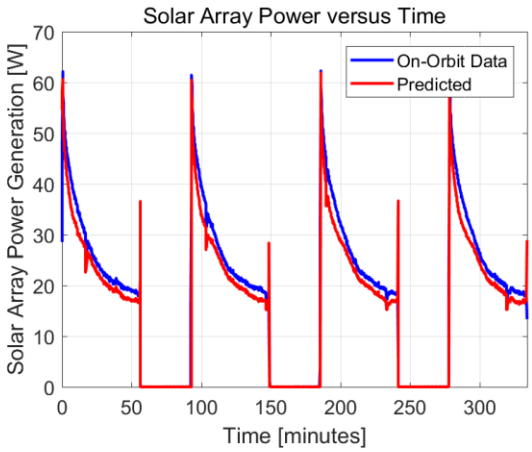

Figure 22: Measured and predicted solar array power over several orbits (different from those in Figure 21).

In parallel with establishing the health of the subsystems, the team began commissioning the payload. The first step was acquiring a full frame image (see Figure 23), which required a few workarounds described in the lessons learned section below. In addition to verifying imager functionality, the full frame image was required for calibration of optical parameters such as focal length, distortion, and alignment relative to the XACT, which are used in the PCS algorithm.

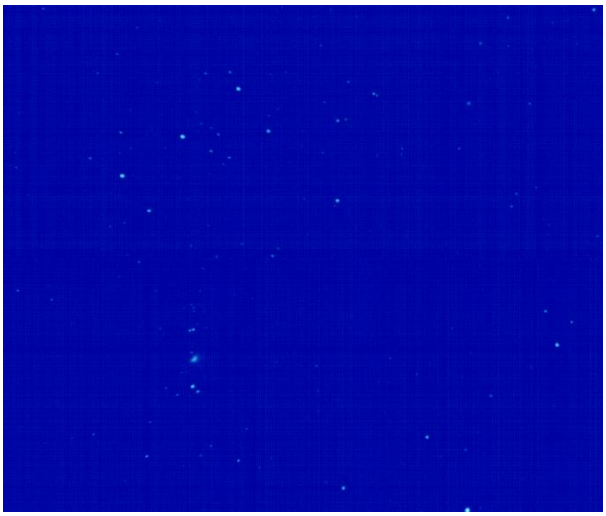

Figure 23: ASTERIA full frame image of the constellation Orion (belt in the upper left quadrant). This image is 2560 by 2160 pixels and covers 11.2° by 9.6°.

Pointing Control Results

ASTERIA has observed several targets to date. This section will describe results for HD 219134, a nearby bright star (V=5.5). These results, including all figures in this section, are from C. M. Pong 2018.[9] Please refer to that publication for additional details on the pointing performance, PCS software, other targets observed, and on-orbit ACS anomalies.

Recall that during observations, the payload operates in windowed mode with up to eight individual windows output every 50 ms. The pointing control algorithm tracks the motion of the star centroids and adjusts the piezo stage position to keep the images stationary. Figure 24 shows the set of windows for HD 219134. The point spread function (PSF) is oversampled and highly aberrated compared to a typical diffraction-limited telescope. This was a necessary tradeoff to obtain acceptable image quality across a very wide field of view. In fact, it presents an advantage for opportunistic science, as the larger PSF mitigates the impact of pixel variation on photometry.

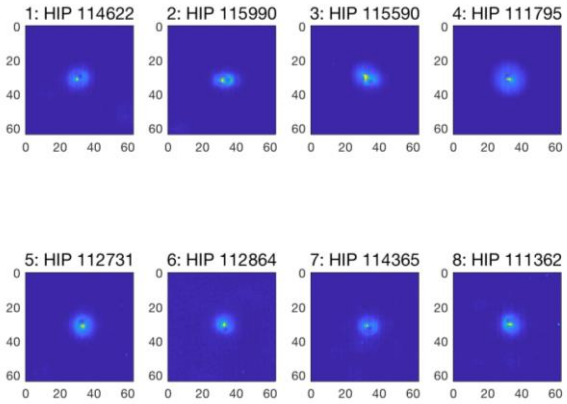

Figure 24: Windowed images of the target star HD 219134 (window 1) and guide stars (windows 2-8).[9] Each window is 64 by 64 pixels.

Figure 25 shows the cross-boresight attitude and pointing errors for a 20-minunte observation of HD 219134. The orange line (pointing error) can be thought of as the path that the target star traces over the imager during the observation while the piezo stage is active. The root mean square value of this error—here termed pointing stability—is better than 0.5 arcseconds over 20 minutes. This corresponds to roughly 1/30th of a pixel and is the best pointing stability achieved to date by a spacecraft of this size (see Figure 1).

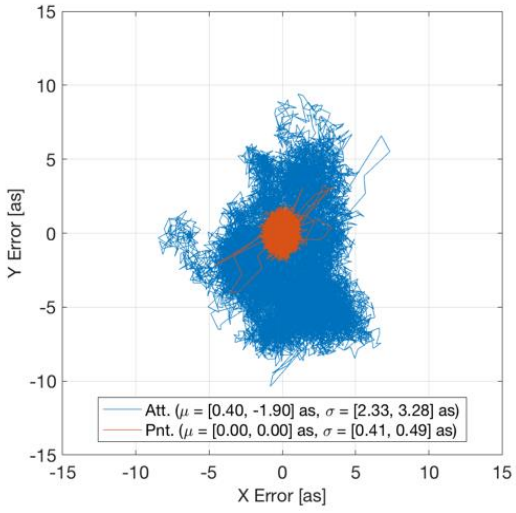

Figure 25: Attitude and pointing error scatter plot for a HD 219134 observation lasting 20 minutes. Pointing stability is better than 0.5 arcseconds RMS over the observation period.[9]

The blue line is calculated by combining the measured pointing error with the recorded piezo stage position to

determine the error that would have resulted if the piezo stage were not moving. See C. M. Pong 2018 for additional discussion of attitude and pointing error.[9]

For this target field, the stars were placed at the same location on the imager during more than 50 observations spanning a 90-day period. Due to data volume limitations, low-level pointing control data (used to verify the pointing performance) were downlinked for only nine observations as of this writing. Calculating the mean pointing error for each observation and taking the root mean square of those mean values yields a pointing repeatability of 1 milliarcsecond RMS over those observations.

Thermal Control Results

During observations, the thermal control system is activated using a set point of 27°C. The reason for the relatively high temperature setting is that control authority is only "one way" (i.e. only heat can be applied, no active cooling) and the imager's own dissipation yields a relatively high steady state temperature. Imaging performance is not degraded with operation at this temperature because the CIS2521 imager has low dark current over the 50 ms integration time.

Figure 26 shows the effect of the optical telescope isolation and active thermal control over many orbits. Each sinusoidal variation corresponds to a single orbit and the spacecraft chassis varies over a range of ±7°C. The Interface Board, which is mounted to the chassis, varies too (±2.5°C) albeit with a lower amplitude thanks to low thermal conductivity material at the mounting interface.

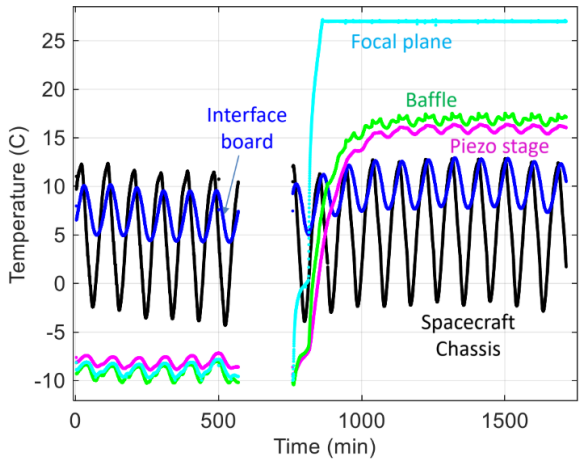

Figure 26: ASTERIA flight data showing temperatures of spacecraft and payload components both before and after thermal control is activated.

The activation of thermal control is clearly visible in Figure 26, causing a step increase in focal plane temperature. Prior to active control, the focal plane, baffle, and piezo stage temperatures oscillate in phase with the chassis, although at a lower amplitude due to the low-conductivity titanium bipods between the OTA and the rest of the spacecraft. During this pre-control period the baffle temperature varies ±1°C and the piezo stage and focal plane both vary ±0.75°C, both very close to thermal model results. Once the control system is activated, the mean focal plane temperature increases to the set point value. Because the imager and thermal control system dissipate heat and are well coupled to the other payload components, the mean temperature of the baffle, piezo stage, and to some extent the spacecraft chassis all experience a corresponding temperature increase. The baffle and piezo stage variation after thermal control is active decrease to ±0.5°C.

Figure 27 shows the temperature at various locations on the focal plane while thermal control is active. For operational reasons related to the pointing control software, the imager undergoes a power cycle before and after each observation. As a result, the internal dissipation momentarily changes, causing the temperature transients visible in the data. Photometric observations are initiated after the transients settle, so there is no impact on opportunistic science data.

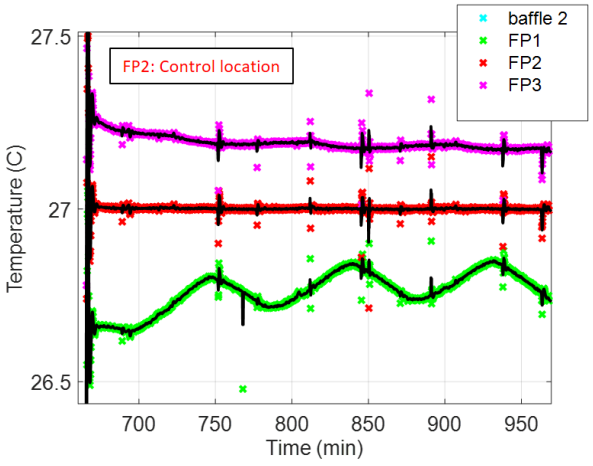

Figure 27: Temperature at three locations on the ASTERIA focal plane while actively controlling the temperature of location 2.

The three temperature sensors referenced in Figure 27 are at three different locations on the back of the imager. The distance between each sensor is small (approximately 10 mm), but clearly there are residual temperature differences between the sensors. This is because the temperate control loop is controlling to the

temperature only at sensor 2. The controller is not currently attempting to null gradients in the system.

Figure 28 shows an expanded view of the temperature reported by focal plane sensor 2 during one of the 20-minute observations. The raw temperature values are recorded every 10 seconds and are shown along with a moving window average over 1 minute. The thermal control loop updates at 0.2 Hz. The measured temperature fluctuations over 20 minutes are within the required tolerance of ±0.01 K and within ±0.005 for most of the samples. This is the best focal plane temperature control achieved to date by a spacecraft this size (see Figure 2).

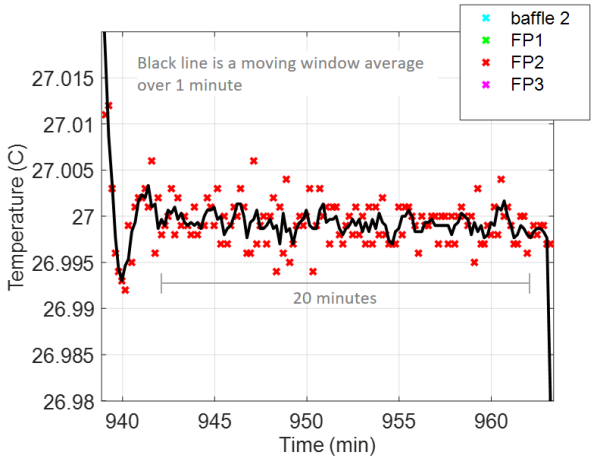

Figure 28: Temperature at one location on the ASTERIA focal plane when actively controlling temperature. The temperature variation is within ±0.01 K over the observation period.

Science Targets

The ASTERIA mission has included opportunistic science both during and after successful completion of the technology demonstration phase. The opportunistic science is focused on transiting exoplanets, i.e. planets that pass in front of the star as seen from the telescope. During transit, a star's measured brightness will drop by a small amount, equal to the planet-to-star area ratio. ASTERIA has a small aperture (60 mm diameter) yet being above the blurring effects of Earth's atmosphere, ASTERIA is capable of high-precision photometry on bright stars. ASTERIA's three primary target stars are 55 Cancri, HD 219134, and Alpha Centauri.

55 Cancri is a nearby Sun-like star (12.5 parsecs, spectral type G8V). 55 Cancri hosts five exoplanets, one of which, 55 Cancri e, is known to transit. 55 Cancri e is a small planet ($2R_{Earth}$) with an 18-hour orbital period.[25,26] ASTERIA observed 55 Cancri in an effort to detect the transit of 55 Cancri e and thereby demonstrate a high level of photometric precision.[27]

HD 219134 is the brightest, nearest star with known transiting exoplanets (V=5.5, 6.5 parsecs). In addition to the two known transiting planets—HD 219134 b and c[28,29]—two additional planets detected via the radial velocity method—HD 219134 d and f—may also transit with probabilities of 13% and 8%, respectively.[28] ASTERIA observed HD 219134 during the predicted transit windows of planets f and d to search for the transits of one or both of these planets.

Alpha Centauri is the closest star system to the Sun and one of the brightest objects in the night sky (V=-0.27, 1.34 parsecs). Both components of the main binary (Alpha Cen A/B) are sun-like (G2V, K1V) and are therefore of intense interest for exoplanet searches. ASTERIA observed Alpha Centauri in order characterize the optical payload's performance for a very bright object and also to search for transit events of as-yet unknown small planets in orbit around either of the binary components. The A/B stars are not separately resolved by ASTERIA's optics, but this does not eliminate the ability to potentially discover small exoplanets should they transit.

Observation Planning

ASTERIA observations take place under a number of constraints that fall into two categories: geometric constraints on the line of sight between the spacecraft and target star, and operational constraints due to technical or safety limitations inherent in the spacecraft subsystems. The key geometric constraints are as follows:

- Observations must take place in eclipse (when ASTERIA is in the Earth's shadow).
- The target star must be at least 20 degrees away from the Moon to minimize stray light.
- The payload boresight must be at least 90 degrees away from spacecraft nadir to avoid stray light from the Earth limb.

Operational constraints are in place to maximize data quality and ensure that observations do not negatively impact spacecraft health and safety. Operational constraints include the following:

- Observations cannot take place during communications passes.

- Observations are limited to a maximum of 30 minutes to avoid overflowing the image buffer in FSW memory.
- To maintain lower limits on the battery state of charge, ASTERIA is not permitted to be oriented with its solar array away from the sun for more than 43 consecutive minutes.
- The ACS/PCS systems require five minutes to slew and settle before beginning to collect science-quality data.
- Observations must avoid reaction wheel zero crossings while also avoiding building up excessive momentum.

In addition to the geometric and operational constraints, observation times for some targets are selected to capture events with known times (e.g. 55 Cancri e transits).

Observation planning begins with selecting a set of orbits between planned communications passes. Typically 10 to 13 orbits per 24-hour period are available for observations. Planning then proceeds through the steps listed below and shown in Figure 29 to generate an observation sequence for uplink to the spacecraft.

Step 1: Generate eclipse times and geometrically constrained access windows to the target star using STK (System Tool Kit by AGI). The geometric constraints identified above are applied. Figure 30 shows eclipse times (black points) and constrained geometric access times (blue circles) for 55 Cancri during ASTERIA's prime mission.

Step 2: Select up to 20 minutes of each constrained geometric access window for observation. ASTERIA performs one set of observations (up to 30 minutes long) per selected orbit. This is often less than the full duration of eclipse, which is typically 30-35 minutes, depending on beta angle.

Step 3: Select a time for the spacecraft to transition from a sun-pointed attitude to an inertial attitude that points the payload at the target star. This slew time must be chosen carefully so that the "off-sun time"—i.e. the time spent with spacecraft solar arrays pointed away from the sun—is less than 43 minutes. Eclipse time, time in a star-pointed attitude, and pre/post observation slews count against off-sun time. The slew time must occur at least 5 minutes before the science observation period begins, to allow slewing and settling.

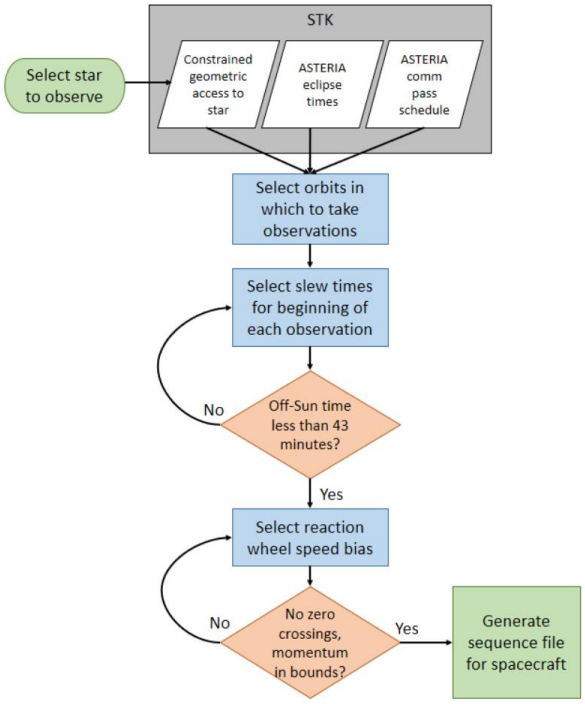

Figure 29: ASTERIA observation planning process.

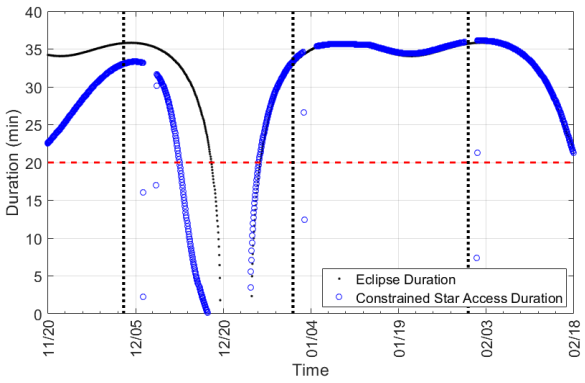

Figure 30: 55 Cancri visibility. The black curve shows eclipse duration for ASTERIA for each orbit during its prime mission. The blue circles show geometrically constrained access duration for each orbit. The vertical black dashed lines show full moons. The access duration drops significantly in the vicinity of each full moon.

Step 4: Check planned slew times and observation durations using a project-developed MATLAB tool that simulates reaction wheel speeds and accumulated momentum throughout the planned set of observations. The reaction wheel speeds may be biased in order to prevent any of the wheels from crossing zero speed during an observation. Reaction wheel zero crossings induce a brief pointing transient and are best avoided for high precision photometric data. [20] If the simulation tool

predicts either reaction wheel speed zero crossings or excessive momentum build-up, the reaction wheel speed bias is adjusted iteratively until there are no zero crossings and maximum accumulated momentum is within bounds.

Step 5: Translate the selected slew times, observation durations, and reaction wheel speed bias into a spacecraft sequence file using another project-developed MATLAB tool.

LESSONS LEARNED

The list of ASTERIA lessons learned is long. Future publications will focus on specific on-orbit anomalies and the steps taken to address them. This section will highlight general findings with particular emphasis on how pre-launch design and testing influenced the operations phase.

The schedule was tight during the final system integration and test period leading to launch. As such, the ASTERIA team prioritized activities to focus on those that would maximize the likelihood of on-orbit success. One lesson learned is that MSTs offer high value during this crucial phase. MSTs took place over a two-week period and provided a forum for relatively long duration FSW testing on the system testbed. This identified two potentially mission-ending software/hardware interactions that were mitigated via FSW updates before delivery. This testing also allowed the team to validate the choices of various watchdog timers and other safety nets that were a critical part of the fault protection design. A significant contributor to the value of the MSTs was the use of a fully functional and flight-like ground data system (GDS), including ground station modem, front-end processor, and GDS software for end-to-end communication with the vehicle over the spacecraft radio. In addition to exposing any technical issues with the integrated system, it provided the team with experience in troubleshooting issues without the rich data provided by the ground umbilical interface.

Another lesson learned is the value of designing flexibility and extensibility into the system with an eye toward operations. By uplinking new parameters, the team has been able to configure which fault monitors are enabled or disabled, which fault responses are linked to which monitors, the limits at which fault conditions are announced, and how long a faulted condition must persist before it triggers a response. This flexibility allowed for an in-flight "tuning" of the fault protection system to address new off-nominal behavior seen in flight. This provides a degree of mitigation against faults that for budget, schedule, or technical reasons cannot be tested before delivery. For example, faults within the XACT caused a temporary loss of attitude control[9] and eventual tripping of a battery voltage monitor. These cases were not observed in ground testing but were addressed on orbit by updating a fault response so that the XACT would be power cycled if the condition occurred again.

Another essential test during the final push to delivery was verification of the ability to update flight software on orbit. This provided a fallback capability for future updates to address corner cases or space environment-related issues that we were unable to test before launch. The ability to update flight software has been exercised twice so far in flight. One of the updates addressed a problem uncovered in the flight software interface between the radio and flight computer. The problems would lead to an expired watchdog timer, which would trigger a flight computer reset. Fault protection worked as intended in these situations, however the FSW update has increased the robustness of the radio interface, decreasing the need for fault protection to intervene and improved operational efficiency.

The ASTERIA flight computer runs the Linux operating system and the flight software incorporates an ability to issue low-level commands directly to the shell. This flexibility has brought several key benefits during mission operations including an ability to diagnose anomalies via command line queries (e.g. ls and grep) and use compression (gzip) to increase effective downlink data volume. The shell interface is also used to send low-level payload commands to mitigate an issue that occasionally precludes imager initialization.

A final lesson learned is the value of continual process improvement during operations. As the mission has progressed, the team has developed various tools and processes to increase efficiency with less staffing. This includes a GitHub-based uplink approval and configuration management process, automated tools for generating observation and engineering sequences, and scripts to parse and organize downlink data. Operational improvements such as actively pointing the spacecraft antenna toward the ground station have increased downlink data throughput. The team continues to investigate options for partially or fully automated passes via the TCL API provided by WTCCS.

FUTURE WORK

ASTERIA is a prototype element of a possible future fleet of up to dozens of satellites. Each satellite would share ASTERIA's precision pointing and thermal control capabilities and operate independently from the others, possibly with larger aperture sizes than ASTERIA's in order to observe fainter stars.

The ultimate goal for the fleet is to monitor dozens of the brightest sun-like stars simultaneously, searching for transiting Earth-size planets in Earth-like (i.e. up to one year) orbits. Because the brightest sun-like stars are distributed across the sky, a single large-aperture telescope is not capable of simultaneous long-duration monitoring of multiple bright stars. This motivates the fleet concept. Each satellite would monitor a single Sun-like target star of interest for as long as possible in order to catch a transit. Nominally, target monitoring would only be interrupted due to geometrical constraints such as Sun, Earth, and Moon keep-out zones. Individual telescopes within the fleet may be tasked to switch between targets to maximize observational coverage as stars move into and out of view.

There are variants on the concept of a space-based precision photometry fleet. One possibility is to have copies of ASTERIA with different detectors to cover bands beyond visible (e.g. near UV, near IR) for distributed multi-color photometry.

CONCLUSION

ASTERIA has advanced the state of the art in pointing and thermal control for small spacecraft. The XACT and PCS achieved a pointing stability of 0.5 arcseconds RMS over 20 minutes and pointing repeatability of 1 milliarcsecond RMS from observation to observation. The thermal control system demonstrated focal plane control of ±0.01 K over 20 minutes.

These achievements were enabled by a simple yet robust fault protection design, thoughtfully tailored system testing, and adaptability during flight operations. The project team—mostly early career employees—received valuable hands-on experience in flight project development and operations that they will carry into future efforts.

Having satisfied its technology demonstration goals, ASTERIA is engaged in an extended mission to look for transiting exoplanets around nearby bright stars. Work is ongoing to improve operational efficiency by enhancing the level of MOS automation. In the future, the technologies developed and lessons learned on ASTERIA may be applied to a fleet of small space telescopes searching for Earth-sized exoplanets. The technology is also applicable to other mission concepts in astrophysics, Earth science, space situational awareness, or any other area in which precision pointing or thermal control are important capabilities.

Acknowledgments

This work was carried out at the Jet Propulsion Laboratory, California Institute of Technology, under a contract with the National Aeronautics and Space Administration. Government sponsorship acknowledged. Reference herein to any specific commercial product, process, or service by trade name, trademark, manufacturer, or otherwise, does not constitute or imply its endorsement by the United States Government or the Jet Propulsion Laboratory, California Institute of Technology.

We acknowledge the contributions of the extended team that supported this project during development and operations, including Len Day, Maria de Soria Santacruz-Pich, Carl Felten, Janan Ferdosi, Kristine Fong, Harrison Herzog, Jim Hofman, David Kessler, Roger Klemm, Tejas Kulkarni, Jules Lee, Jason Munger, Lori Moore, Esha Murty, Chris Shelton, David Sternberg, Rob Sweet, Kerry Wahl, Jacqueline Weiler, Thomas Werne, and Shannon Zareh

We recognize the JPL line organization and technical mentors for the expertise they provided throughout the project. We are grateful for the leadership of Sarah Gavit, who oversaw ASTERIA within the Engineering and Science Directorate at JPL. We also thank Daniel Coulter and Leslie Livesay in the JPL Astronomy and Physics Directorate for their support.

We thank Brice-Olivier Demory at the University of Bern for his guidance on target star selection and his indispensable expertise on photometric data processing and analysis.

Finally, we recognize the contributions of the student operators, technical staff, and program management at Morehead State University, including Tobias Gedenk, Chloe Hart, Sarah Wilczewski, Alex Roberts, Bob Kroll, Michael Combs, and Benjamin Malphrus. Their flexibility, responsiveness, and enthusiasm has been indispensable to our mission.

References

1. M.W. Smith, et al., “ExoplanetSat: Detecting transiting exoplanets using a low-cost CubeSat platform,” *Proceedings of SPIE*, Vol. 7731 (2010).
2. C. M Pong, et al., “Achieving high-precision pointing on ExoplanetSat: Initial feasibility analysis,” *Proceedings of SPIE*, Vol. 7731 (2010).
3. C. M. Pong, et al., “One-Arcsecond Line-of-Sight Pointing Control on ExoplanetSat,” *Guidance and Control 2011*, Vol. 141 of Advances in the Astronautical Sciences, AAS, Univelt, Inc., Breckenridge, CO, February 2011, pp. 147–166.
4. M. W. Smith, et al. “The ExoplanetSat Mission to Detect Transiting Exoplanets with a CubeSat Space Telescope,” *Small Satellite Conference*,

AIAA/USU, Utah State University Research Foundation, Logan, UT, August 2011, pp. 1–9.

5. C. M. Pong, et al., "High-Precision Pointing and Attitude Determination and Control on ExoplanetSat," *AIAA Guidance, Navigation, and Control Conference*, Minneapolis, MN, August 2012, pp. 1–24.
6. M. Knapp, et al., "ExoplanetSat: High Precision Photometry for Exoplanet Transit Detections in a 3U CubeSat," *63rd International Astronautical Congress*, IAF, Naples, Italy, October 2012, pp. 1–12.
7. C. M. Pong, et al., "Three-Degree-of-Freedom Testing of Attitude Determination and Control Algorithms on ExoplanetSat," *Guidance and Control 2014*, Vol. 151 of Advances in the Astronautical Sciences, AAS, Univelt, Inc., Breckenridge, CO, February 2014, pp. 285–307.
8. C. M. Pong, *High-Precision Pointing and Attitude Estimation and Control Algorithms for Hardware-Constrained Spacecraft*, Doctor of Science thesis, Massachusetts Institute of Technology, Cambridge, MA, May 2014.
9. Pong, C. M., "On-Orbit Performance & Operation of the Attitude & Pointing Control Subsystems on ASTERIA," *Proceedings of the AIAA/USU Conference on Small Satellites*, Poster Session 1, SSC18-PI-34.
10. L. Duband, et al., "In-Flight Performance of the HERSCHEL Sorption Coolers – One Year of Operations," *Cryocoolers 16* (2011).
11. S. Carey, et al., "Stability of the Infrared Array Camera for the Spitzer Space Telescope," *Proc SPIE*, Vol. 7010 (2008).
12. D. G. Koch, et al., "*Kepler Mission* Design, Realized Photometric Performance, and Early Science," Vol. 713, No. 2 (2010).
13. R. M. Cutri, et al., "Explanatory Supplement to the WISE All-Sky Data Release Products," http://wise2.ipac.caltech.edu/docs/release/allsky/expsup/sec3_2.html
14. G. R. Ricker et al., "The Transiting Exoplanet Survey Satellite" *arXiv:1406.0151 [astro-ph.EP]* (2014).
15. M. Auvergine, et al., "The CoRoT satellite in flight: description and performance," *Astronomy & Astrophysics*, Vol. 506, No. 1 (2009).
16. A. Fortier, et al., "CHEOPS: a space telescope for ultra-high precision photometry of exoplanet transits," *Proc SPIE*, Vol. 9143 (2014).
17. G. Walker, et al., "The MOST Asteroseismology Mission: Ultraprecise Photometry from Space," *Publications of the Astronomy Society of the Pacific*, Vol. 115, p. 1023 (2003).
18. J. C. T. Cheng, et al., "The BRITE Constellation Space Telescope Design and Test of a Wide Field, High Resolution, Low Noise Optical Telescope for a Nanosatellite Constellation," *Proceedings of the AIAA/USU Conference on Small Satellites*, SSC11-I-1 (2011).
19. Bocchino, R.L. et al. 2018. "F Prime: An Open-Source Framework for Small-Scale Flight Software Systems," *Proceedings of the AIAA/USU Conference on Small Satellites*, Advanced Technologies II, SSC-18-XII-04.
20. CubeSat Design Specification (CDS), Revision 13, *The CubeSat Program, Cal Poly San Luis Obispo*, 2014.
21. B. Malphrus, M. Combs, J. Kruth, N. Fite, B. Twiggs, R. Schulze, "A University-Based Ground Station: The 21 m Antenna at Morehead State University," *AIAA SpaceOps Conference*, 25-30 April 2010, Huntsville, Alabama.
22. K. R. Fields, "Mass Property Measurements of the Mars Science Laboratory Rover," *72nd International Conference on Mass Properties Engineering*, May 2013.
23. I. Heinrichsen and E. L. Wright, "The Mission Operations System for Wide-field Infrared Survey Explorer (WISE)", *Proc. SPIE*, Vol. 5270, pp. C-1 to C-9 (2006).
24. J. Trimble, "Reconfigurable Software for Mission Operations," *AIAA SpaceOps Conference*, 5-9 May 2014, Pasadena, California.
25. B.-O. Demory et al., "Detection of a transit of the super-Earth 44 Cancri e with warm Spitzer," *Astronomy and Astrophysics* 553, A114 (2011).
26. J. N. Winn et al., "A Super-Earth Transiting a Naked-Eye Star," *The Astrophysical Journal Letters*, Vol. 737, No. 1 (2011).
27. M. Knapp et al. (2018), *in preparation*.
28. M. Gillion et al., "Two massive rocky planets transiting a K-dwarf 6.5 parsecs away," *Nature Astronomy*, 1(3), 0056 (2017).
29. F. Motalebi et al., "The HARPS-N Rocky Planet Search: I. HD 219134b: A transiting rocky planet in a multi-planet system at 6.5 pc from the Sun," *Astronomy & Astrophysics*, 584, A72 (2015).